Supporting Information

Coarse-grained Reduced $Mo_xTi_{1-x}Nb_2O_{7+x}$ Anodes for High-Rate Lithium-ion Batteries

Lijiang Zhao [a], Shitong Wang [b], Yanhao Dong [b,*], Wei Quan [e], Fei Han [b], Yimeng Huang [c], Yutong Li [d], Xinghua Liu [a], Mingda Li [b], Zhongtai Zhang [d], Junying Zhang [a,**], Zilong Tang [d,***], and Ju Li [b, c,*]

[a] Key Laboratory of Micro-nano Measurement, Manipulation and Physics (Ministry of Education), School of Physics, Beihang University, Beijing 100191, China.

[b] Department of Nuclear Science and Engineering, Massachusetts Institute of Technology, Cambridge, Massachusetts 02139, USA

[c] Department of Materials Science and Engineering, Massachusetts Institute of Technology, Cambridge, Massachusetts 02139, USA

[d] State Key Lab of New Ceramics and Fine Processing, School of Materials Science and Engineering, Tsinghua University, Beijing 100084, China

[e] China Automotive Battery Research Institute Co., Ltd., Beijing 101407, China

General Research Institute for Nonferrous Metals, Beijing 100088, China

***** Corresponding author.

****** Corresponding author.

******* Corresponding author.

E-mail addresses: zjy@buaa.edu.cn (Junying Zhang), tzl@tsinghua.edu.cn (Zilong Tang), dongyh@mit.edu (Yanhao Dong) , liju@mit.edu (Ju Li)

Supplementary Figures S1~S14

Supplementary Tables S1~S8

Supplementary References S1~S31

Supplementary Figures

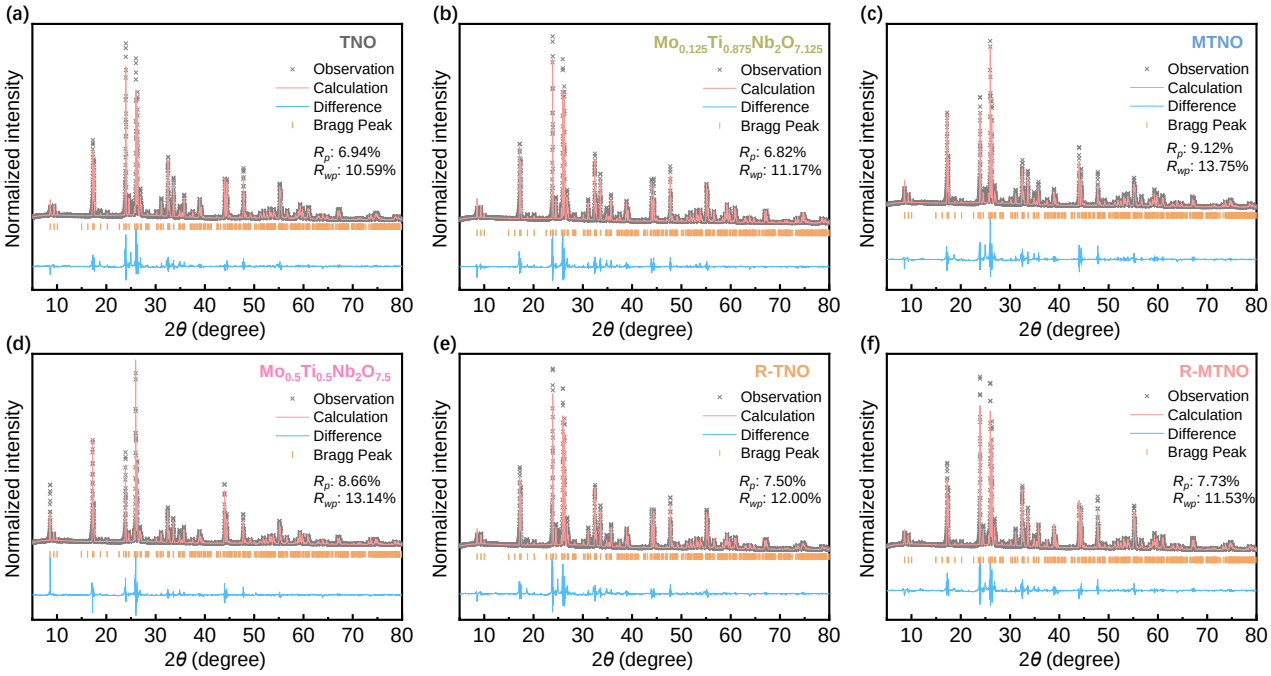

Fig. S1. XRD pattern as well as the Rietveld refinement analysis of (a) TNO, (b) $Mo_{0.125}Ti_{0.875}Nb_2O_{7.125}$, (c) MTNO, (d) $Mo_{0.5}Ti_{0.5}Nb_2O_{7.5}$, (e) R-TNO and (f) R-MTNO. More details are shown in Table S2.

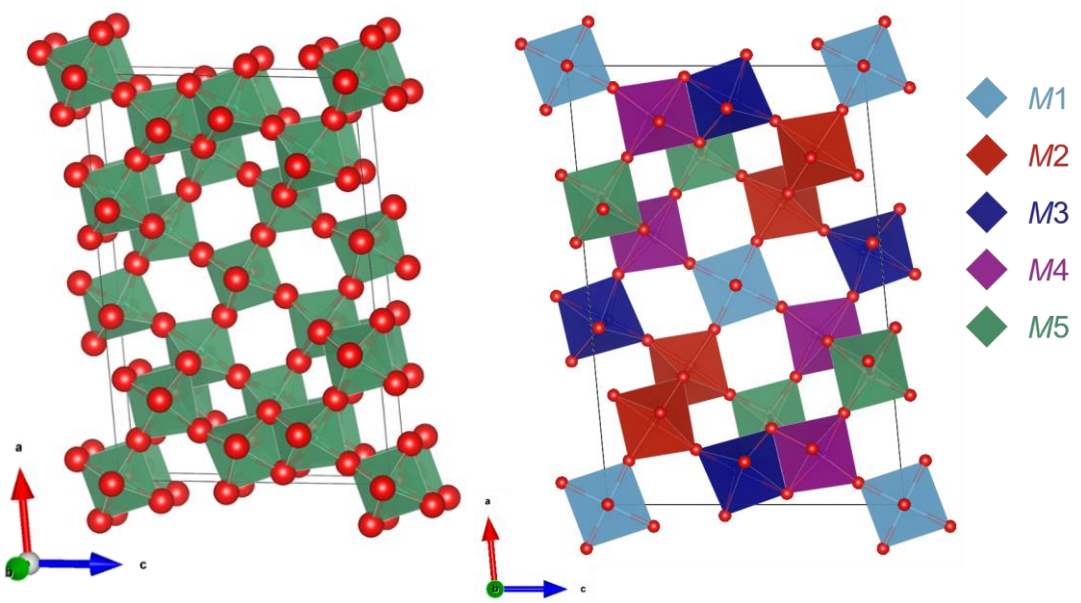

Fig. S2. Crystal structure (left) and schematic polyhedron packing (right) of $TiNb_2O_7$. More details about atomic occupancy information are shown in Table S3.

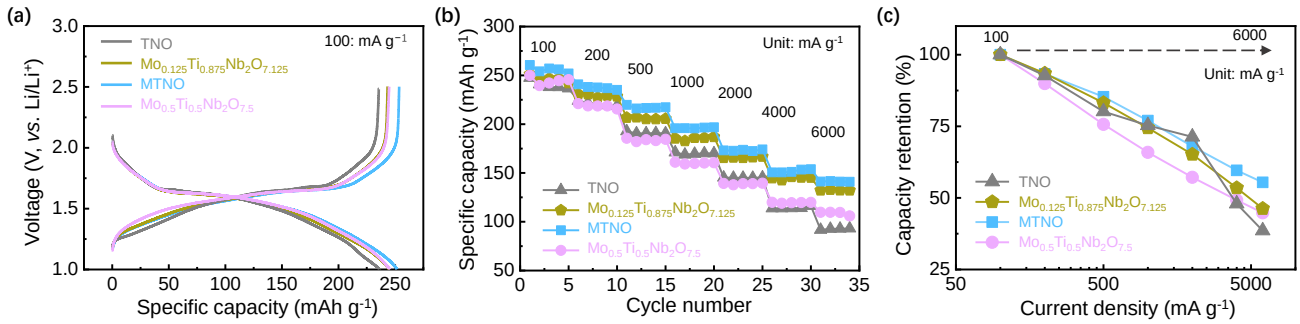

Fig. S3. (a) Galvanostatic discharge/charge profiles, (b) Rate performances, (c) rate capacity retention of TNO, $Mo_{0.125}Ti_{0.875}Nb_2O_{7.125}$, MTNO, and $Mo_{0.5}Ti_{0.5}Nb_2O_{7.5}$.

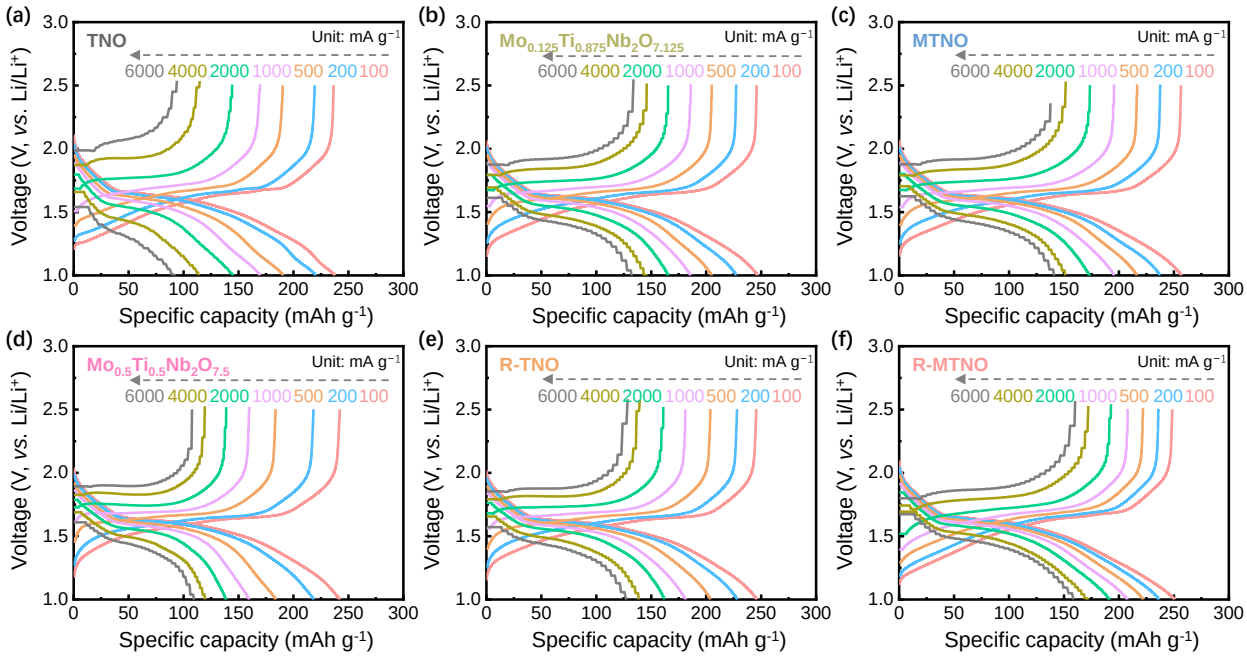

Fig. S4. Galvanostatic discharge/charge profiles at different current densities of (a) TNO, (b) $Mo_{0.125}Ti_{0.875}Nb_2O_{7.125}$, (c) MTNO, (d) $Mo_{0.5}Ti_{0.5}Nb_2O_{7.5}$, (e) R-TNO and (f) R-MTNO.

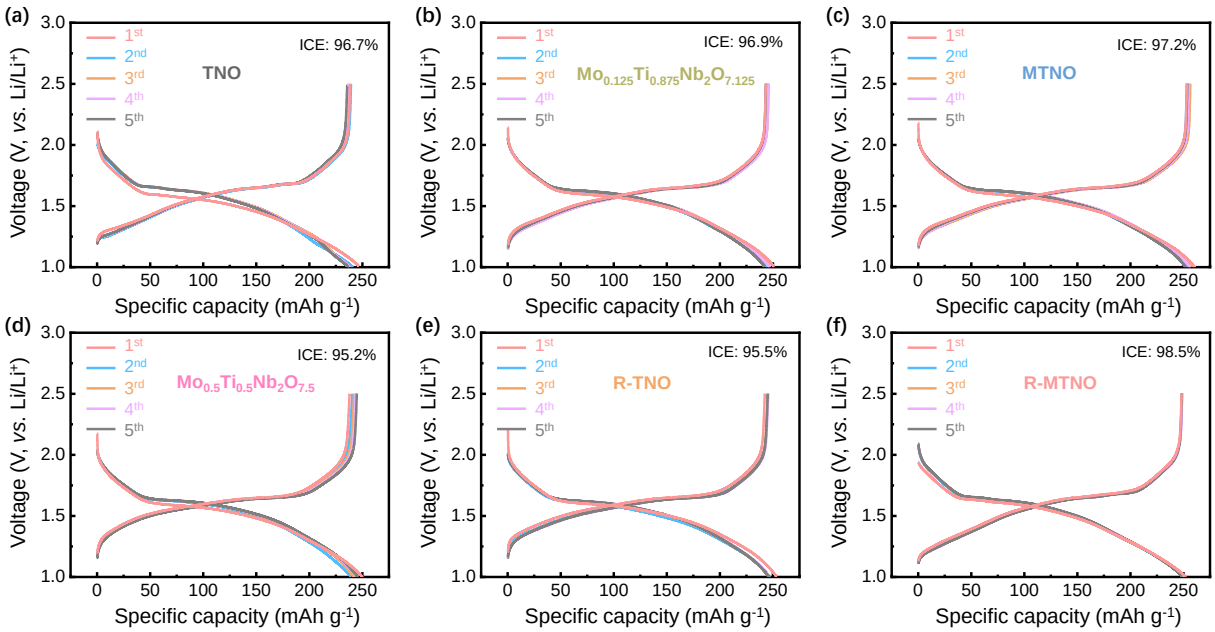

Fig. S5. Galvanostatic discharge/charge profiles at 100 mA g^{-1} for the first five cycles of (a) TNO, (b) $Mo_{0.125}Ti_{0.875}Nb_2O_{7.125}$, (c) MTNO, (d) $Mo_{0.5}Ti_{0.5}Nb_2O_{7.5}$, (e) R-TNO and (f) R-MTNO.

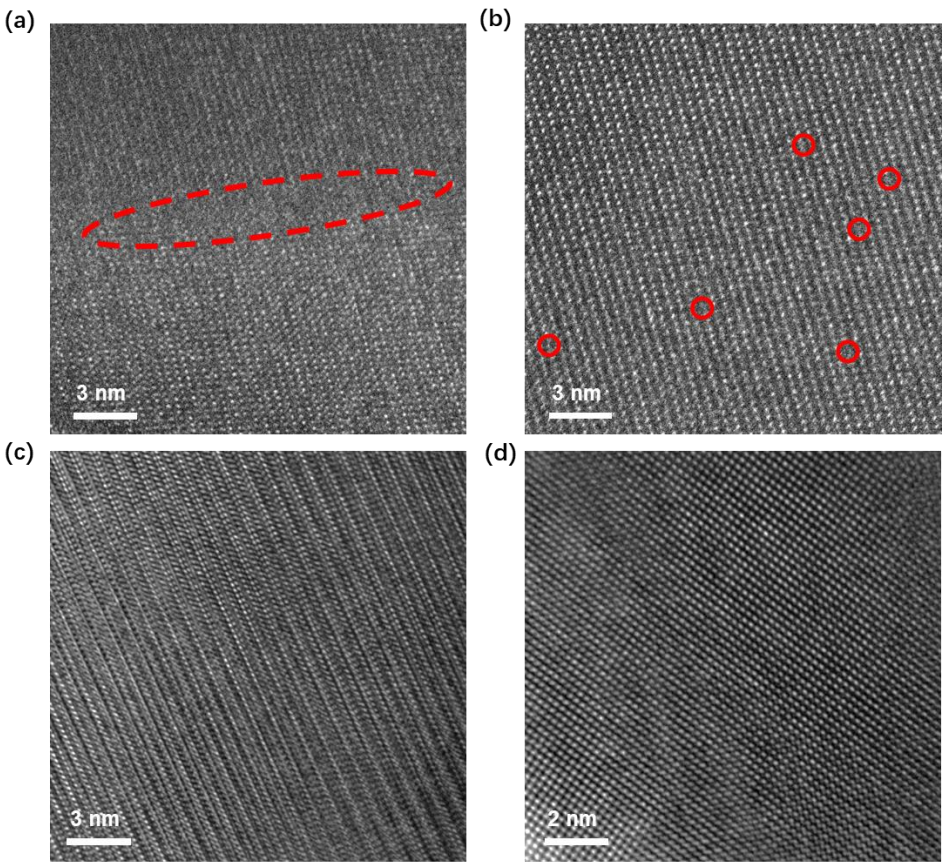

Fig. S6. HRTEM images of (a, b) R-MTNO showing more disorders and defect than (c, d) MTNO.

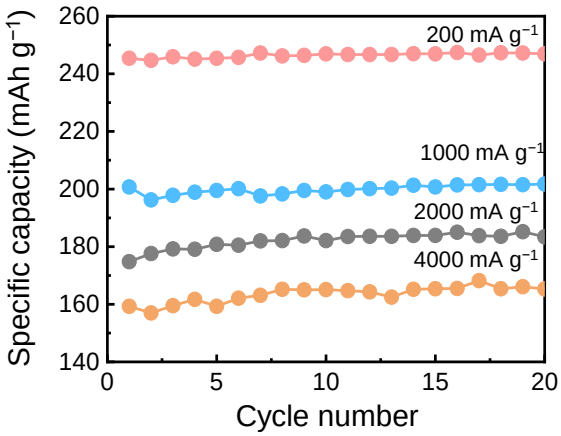

Fig. S7. Cycling performance of R-MTNO at 200, 1000, 2000 and 4000 mA g^{-1} for the first 20 cycles.

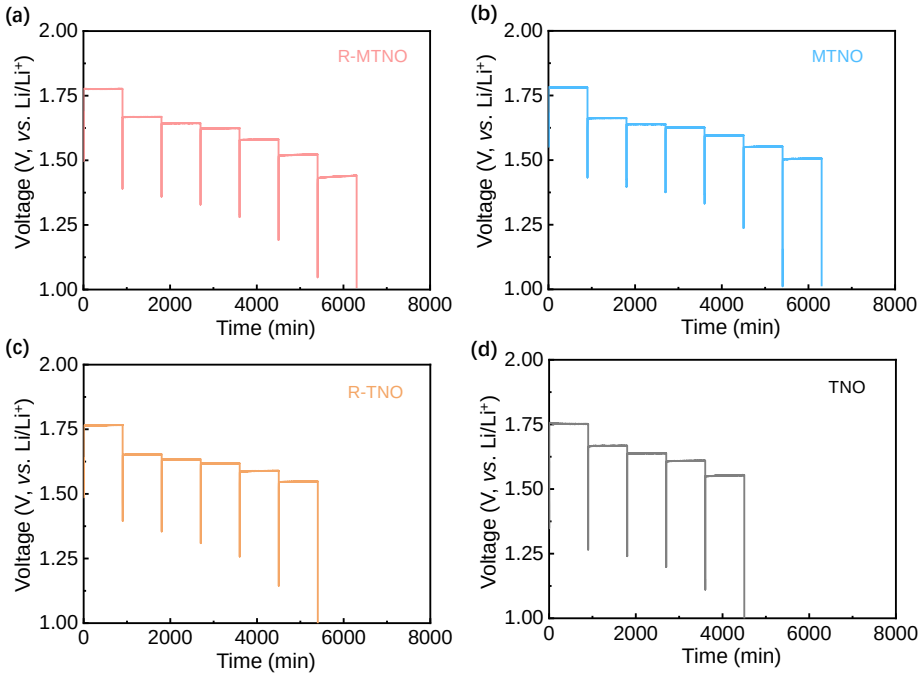

Fig. S8. GITT curves at 4000 mA g^{-1} for R-MTNO, MTNO, R-TNO and TNO electrodes.

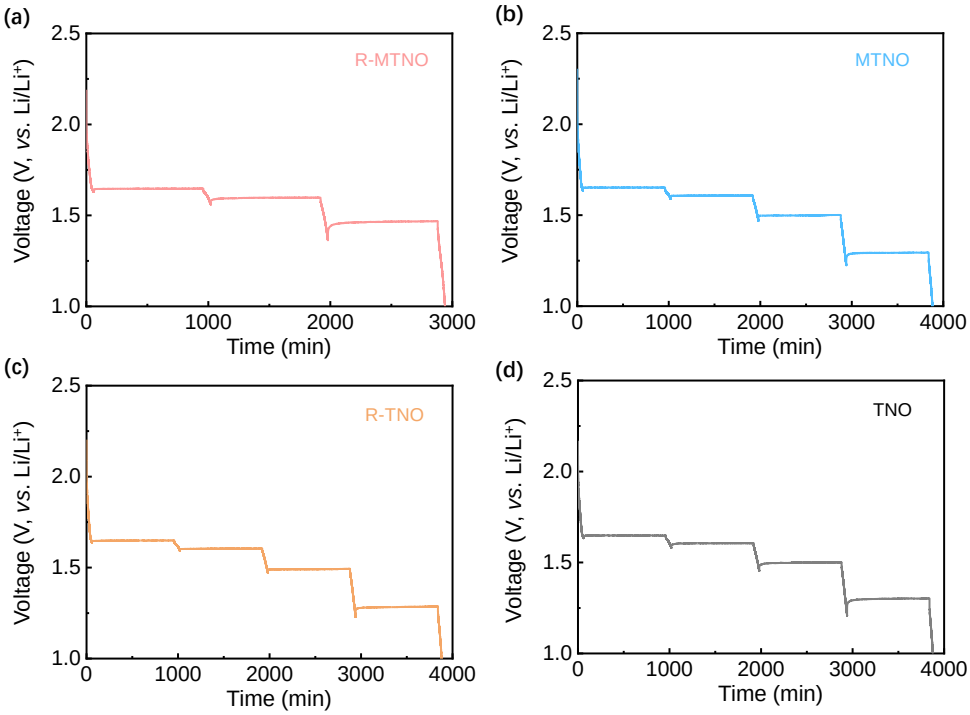

Fig. S9. GITT curves at 50 mA g^{-1} for R-MTNO, MTNO, R-TNO and TNO electrodes.

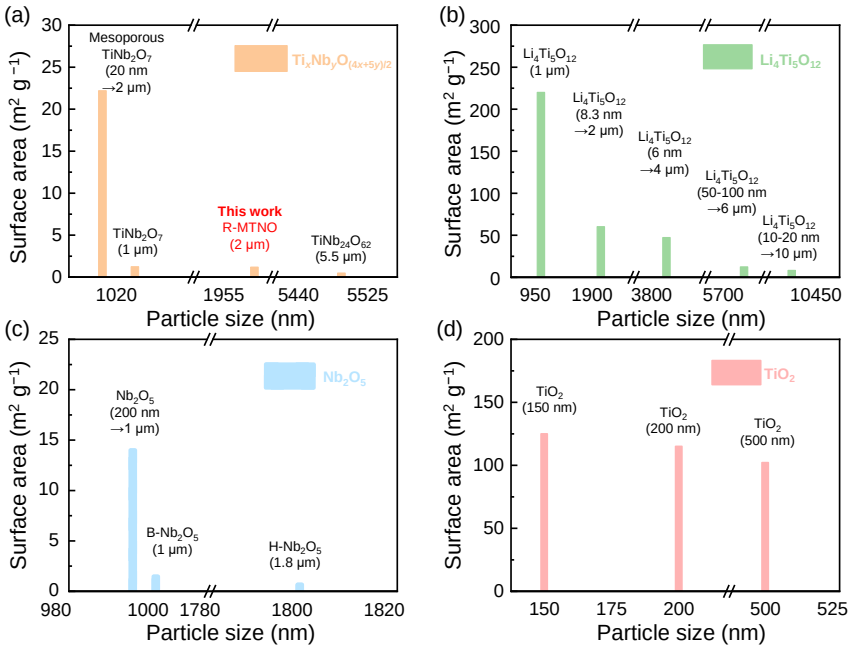

Fig. S10. Particle size versus specific surface area of representative $Ti_xNb_yO_{(4x+5y)/2}$, Nb_2O_5, $Li_4Ti_5O_{12}$ and TiO_2 electrodes. More details are shown in **Table S5**.

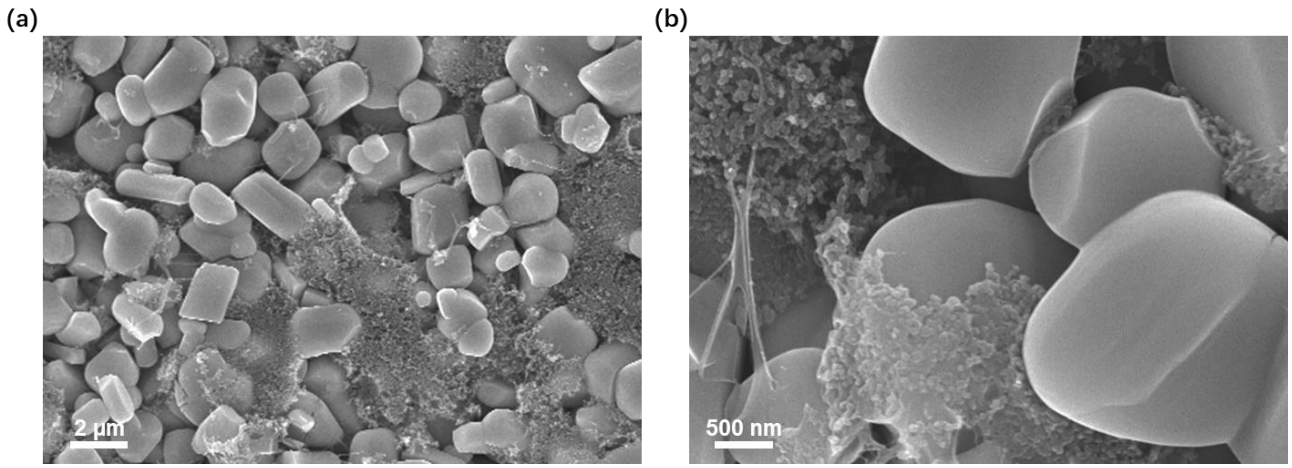

Fig. S11. SEM images for R-MTNO electrodes before cycling.

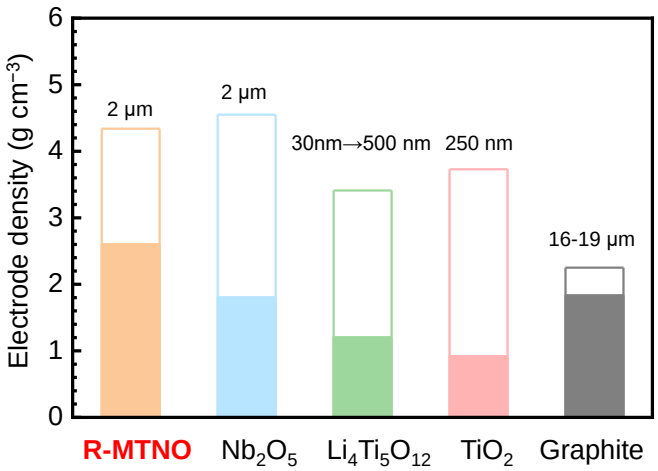

Fig. S12. Particle size and electrode density of $Mo_xTi_{1-x}Nb_2O_{7+x}$, representative Nb_2O_5, $Li_4Ti_5O_{12}$ and TiO_2 and graphite. Solid bar represents real density; integral hollow bar represents theoretical density. More details are shown in **Table S6**.

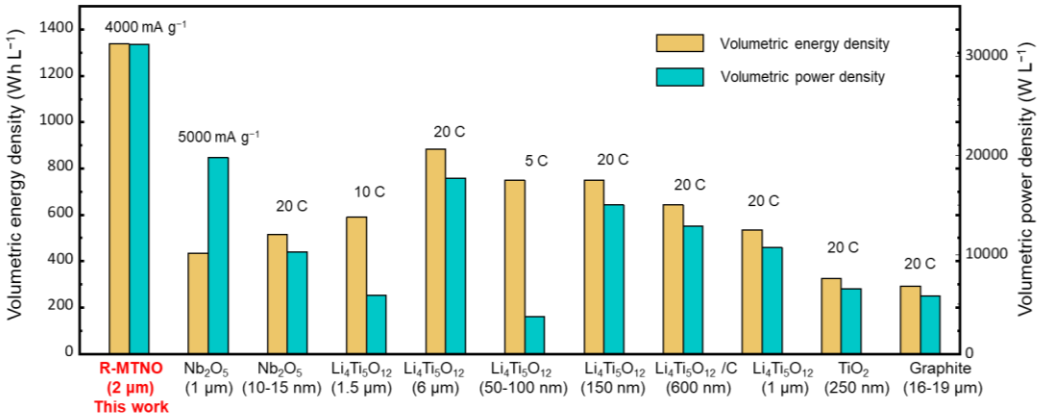

Fig. S13. Volumetric energy densities and power densities based on the anode (without current collector) of $Mo_xTi_{1-x}Nb_2O_{7+x}$, representative Nb_2O_5, $Li_4Ti_5O_{12}$, TiO_2, and graphite by using $LiNi_{0.5}Mn_{1.5}O_4$ as the reference cathode. More details are shown in **Table S7**.

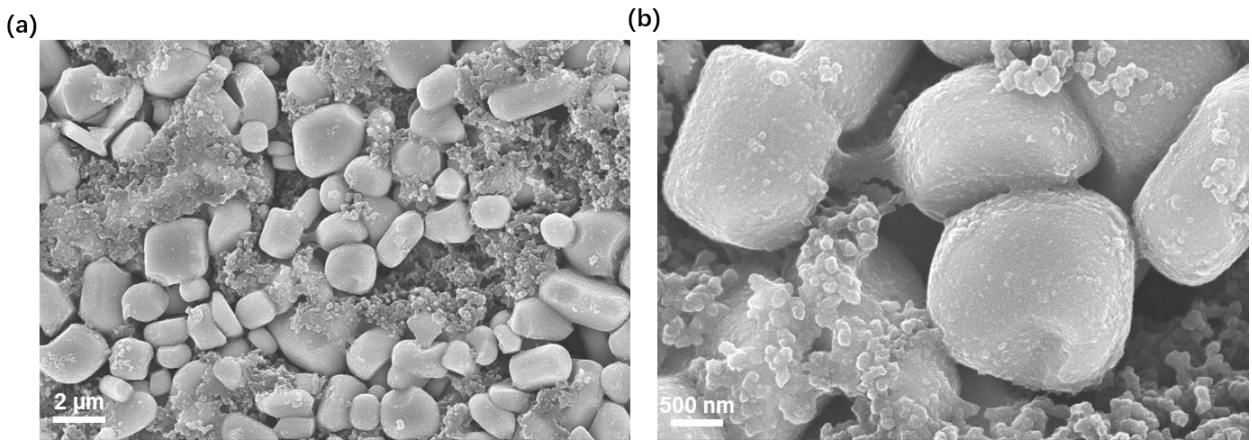

Fig. S14. SEM images for R-MTNO electrodes after 500 cycles at 2000 mA g^{-1}.

Supplementary Tables

Table S1 Compositions of TNO, $Mo_{0.125}Ti_{0.875}Nb_2O_{7.125}$, MTNO, $Mo_{0.5}Ti_{0.5}Nb_2O_{7.5}$ measured by inductively coupled plasma atomic emission spectroscopy (ICP-MS).

Targeted composition	Measured composition
$TiNb_2O_7$ (TNO)	$Ti_{1.03}Nb_{1.97}O_{6.99}$
$Mo_{0.125}Ti_{0.875}Nb_2O_{7.125}$	$Mo_{0.11}Ti_{0.89}Nb_{1.99}O_{7.11}$
$Mo_{0.25}Ti_{0.75}Nb_2O_{7.25}$ (MTNO)	$Mo_{0.30}Ti_{0.73}Nb_{1.97}O_{7.29}$
$Mo_{0.5}Ti_{0.5}Nb_2O_{7.5}$	$Mo_{0.65}Ti_{0.47}Nb_{1.88}O_{7.59}$

Table S2 Rietveld refinement results TNO, $Mo_{0.125}Ti_{0.875}Nb_2O_{7.125}$, MTNO, $Mo_{0.5}Ti_{0.5}Nb_2O_{7.5}$, R-TNO and R-MTNO. (Because of the structural complexity, the present powder diffraction data do not allow accurate refinements for atomic occupancies.)

Materials	*a* (Å)	*b* (Å)	*c* (Å)	α (°)	β (°)	γ (°)
TNO	17.68	3.80	11.90	90.00	95.32	90.00
$Mo_{0.125}Ti_{0.875}Nb_2O_{7.125}$	17.68	3.80	11.90	90.00	95.32	90.00
MTNO	17.68	3.80	11.89	90.00	95.32	90.00
$Mo_{0.5}Ti_{0.5}Nb_2O_{7.5}$	17.68	3.80	11.90	90.00	95.31	90.00
R-TNO	17.68	3.80	11.90	90.00	95.32	90.00
R-MTNO	17.67	3.80	11.89	90.00	95.33	90.00

Table S3 Atomic occupancy information of $TiNb_2O_7$[S1].

Atom	*x*	*y*	*z*	Occupancy	Site	Polyhedron
Nb1	0.00000	0.00000	0.00000	0.909	2*a*	*M*1
Ti1	0.00000	0.00000	0.00000	0.091	2*a*	*M*1
Nb2	0.18528	0.00000	0.17993	0.798	4*i*	*M*2
Ti2	0.18528	0.00000	0.17993	0.202	4*i*	*M*2
Nb3	0.07842	0.00000	-0.55844	0.643	4*i*	*M*3
Ti3	0.07842	0.00000	-0.55844	0.357	4*i*	*M*3
Nb4	0.88938	0.00000	0.25857	0.727	4*i*	*M*4
Ti4	0.88938	0.00000	0.25857	0.273	4*i*	*M*4
Nb5	0.29286	0.00000	-0.07479	0.376	4*i*	*M*5
Ti5	0.29286	0.00000	-0.07479	0.624	4*i*	*M*5
O1	0.17350	0.00000	-0.42330	1.000	4*i*	/
O2	0.37287	0.00000	-0.20690	1.000	4*i*	/
O3	0.59702	0.00000	-0.02520	1.000	4*i*	/
O4	0.79131	0.00000	0.17440	1.000	4*i*	/
O5	0.24932	0.00000	0.05400	1.000	4*i*	/
O6	0.70916	0.00000	0.70590	1.000	4*i*	/
O7	0.89988	0.00000	-0.08510	1.000	4*i*	/
O8	0.02523	0.00000	-0.39200	1.000	4*i*	/
O9	0.87451	0.00000	0.68530	1.000	4*i*	/
O10	0.50000	0.00000	0.50000	1.000	2*b*	/
O11	0.04964	0.00000	-0.14790	1.000	4*i*	/

Table S4 Specific surface area and first-cycle Coulombic efficiency of R-MTNO, MTNO, R-TNO and TNO.

Materials	Specific surface area (m^2 g^{-1})	First-cycle Coulombic efficiency (%)
R-MTNO	1.1	98.5
MTNO	1.5	97.2
R-TNO	1.5	95.5
TNO	1.0	96.7

Table S5 Particle size versus specific surface area of representative $Ti_xNb_yO_{(4x+5y)/2}$, Nb_2O_5, $Li_4Ti_5O_{12}$ and TiO_2 electrodes.

Materials	Particle size (μm)	Specific surface area ($m^2\ g^{-1}$)	Refs
R-MTNO	2.0	1.2	This work
Porous $TiNb_{24}O_{62}$	5.5	0.5	[S2]
$TiNb_2O_7$	1.5	1.3	[S3]
Mesoporous $TiNb_2O_7$	1.0	22.2	[S3]
H-Nb_2O_5	1.8	0.7	[S4]
B-Nb_2O_5	1.2	1.5	[S4]
Nb_2O_5 microsphere	1.0	14.0	[S5]
TiO_2	0.5	102.1	[S6]
TiO_2	0.2	115.0	[S7]
TiO_2	0.2	125.0	[S8]
Carbon-coated $Li_4Ti_5O_{12}$	10.0	8.1	[S9]
$Li_4Ti_5O_{12}$	6.0	12.1	[S10]
Porous $Li_4Ti_5O_{12}$	4.0	51.3	[S11]
Mesoporous $Li_4Ti_5O_{12}$	2.0	60.2	[S12]
$Li_4Ti_5O_{12}$ microspheres	1.0	220.0	[S13]

Table S6 Particle size and electrode density of $Mo_xTi_{1-x}Nb_2O_{7+x}$, representative Nb_2O_5, $Li_4Ti_5O_{12}$ and TiO_2 and graphite.

Materials	Particle size (μm)	Electrode density (g cm^{-3})	Refs
R-MTNO	2.0	2.6	This work
Nb_2O_5	2.0	1.8[a]	[S4]
$Li_4Ti_5O_{12}$	0.8~3.0	2.0	[S14]
TiO_2	0.3[b]	0.9	[S15]
Graphite	16~19	1.8	[S16]

a: Tap density of the material.
b: The average length and diameter are 2 μm and 0.3 μm, respectively.

Table S7 Electrochemical comparison table considering the particle size, specific surface area, electrode densities, initial CE, volumetric energy density and volumetric power density among $Mo_xTi_{1-x}Nb_2O_{7+x}$ and representative Nb_2O_5, $Li_4Ti_5O_{12}$, TiO_2 and graphite. The electrode compositions (mass ratio of active materials: conductive carbon: binder (binder)) are listed for references.

Materials	Surface area ($m^2\ g^{-1}$)	Electrode composition	Electrode density ($g\ cm^{-3}$)	Initial CE (%)	High-rate capacity ($mAh\ g^{-1}$)	Volumetric energy density [$Wh\ L^{-1}$]	Volumetric power density [$W\ L^{-1}$]	Refs
R-MTNO	**1.1**	**90:5:2.5:2.5**	**2.6**	**99**	**192 (2000 mA g^{-1})**	**1338**	**31200**	**This work**
MTNO	**1.5**	**90:5:2.5:2.5**	**2.6**	**97**	**173 (2000 mA g^{-1})**	**1179**	**31200**	**This work**
R-TNO	**1.5**	**90:5:2.5:2.5**	**2.6**	**96**	**161 (2000 mA g^{-1})**	**1080**	**31200**	**This work**
TNO	**1.0**	**90:5:2.5:2.5**	**2.6**	**97**	**145 (2000 mA g^{-1})**	**888**	**31200**	**This work**
Nb_2O_5 (150 nm→1 μm)	22.4	80:10:10	≈1.5[a]	92[b]	140 (2000 mA g^{-1})	436	19800	[S5]
Nb_2O_5 (10~15 nm pressed)	83.0	85:15	1.5	90[b]	130 (20 C)	515	10296	[S17]
Carbon-coated $Li_4Ti_5O_{12}$ (10~20 nm→1.5 μm)	3.1	80:10:10	1.3[c]	97[b]	110 (10 C)	590	5896	[S18]
$Li_4Ti_5O_{12}$ (50~100 nm→6 μm)	12.1	80:10:10	1.2[c]	96[b]	165 (20 C)	884	17688	[S10]
$Li_4Ti_5O_{12}$ nanoclusters (50~100 nm)	142.0	80:10:10	0.8[c]	97[b]	140 (5 C)	750	3752	[S19]
$Li_4Ti_5O_{12}$ (150 nm)	46.4	80:10:10	1.2[c]	N/A	140 (20 C)	750	15008	[S20]
$Li_4Ti_5O_{12}$ /C (30 nm→600 nm)	8.6	80:10:10	1.2[c]	N/A	120 (20 C)	643	12864	[S21]
$Li_4Ti_5O_{12}$ microspheres (1 μm)	20.0	80:10:10	≈1.2[a, c]	84[b]	100 (20 C)	536	10720	[S22]
TiO_2 (250 nm)	N/A	80:10:10	0.92	84[b]	200 (0.17 C) 130 (20 C)	327	6530	[S15, 23]
Graphite (16~19 μm)	2.0	92:3:5	1.83	94	36 (20 C)	293	5857	[S16, 24]

a: Estimated by specific surface area.
b: Calculated from the initial voltage capacity curve.
c: Tap density of the material. The calculation of volumetric energy density and power density was based on the electrode density of commercialized $Li_4Ti_5O_{12}$ (2.0 g cm^{-3}).
d: The volumetric energy density and volumetric power density were calculated by the following equations (for the average voltage, we assume charge voltage of 4.9 V for $LiNi_{0.5}Mn_{1.5}O_4$ cathode):

$$\text{Volumetric energy density } (Wh\ L^{-1}) = \frac{(\text{Cell capacity}) \times (\text{Average voltage})}{(\text{Electrode area}) \times (\text{Thickness of anode including active materials, binder and carbon black})}$$

$$\text{Volumetric power density } (W\ L^{-1}) = \frac{(\text{Cell capacity}) \times (\text{Average voltage})}{(\text{Discharging time of anode}) \times (\text{Electrode area}) \times (\text{Thickness of anode including active materials, binder and carbon black})}$$

Table S8 Electrochemical comparison table considering the mass loading, particle size, rate capability and cyclability among recent reported $Ti_xNb_yO_{(4x+5y)/2}$ electrodes.

Materials	Mass loading (mg cm^{-2})	Particle size	Rate capability (mAh g^{-1})	Cyclability (mAh g^{-1})	Refs
R-MTNO	**1~2**	**2 μm**	**158 (6000 mA g^{-1})**	**500 cycles (2000 mA g^{-1}, 75%)**	**This work**
MTNO	**1~2**	**2 μm**	**141 (6000 mA g^{-1})**	**500 cycles (2000 mA g^{-1}, 58%)**	**This work**
R-TNO	**1~2**	**2 μm**	**126 (6000 mA g^{-1})**	**500 cycles (2000 mA g^{-1}, 65%)**	**This work**
TNO	**1~2**	**2 μm**	**92 (6000 mA g^{-1})**	**500 cycles (2000 mA g^{-1}, 29%)**	**This work**
$TiNb_2O_7$	1~1.2	100 nm	150 (20 C)	50 cycles (1 C, 90%)	[S25]
$Ti_2N_{10}O_{29-x}$@C	2	50 nm	200 (20 C)	500 cycles (10 C, 98.7%)	[S26]
$TiNb_2O_7$ /C	1.6~1.8	800 nm	194 (10 C)	500 cycles (5 C, 47%)	[S27]
$TiNb_2O_7$	N/A	100 nm→3 μm	125 (10 C)	500 cycles (10 C, 73%)	[S28]
$Ti_2Nb_{10}O_{29}$	N/A	2 μm	120 (20 C)	800 cycles (10 C, 85%)	[S29]
$TiNb_2O_7$	N/A	100 nm	230 (20 C)	1000 cycles (10 C, 81%)	[S30]
$TiNb_2O_7$	1.5	1 μm	128 (20 C)	500 cycles (10 C, 32%)	[S3]
$TiNb_{24}O_{62}$	N/A	50 nm→2 μm	181 (20 C)	500 cycles (10 C, 90.5%)	[S2]
$TiNb_2O_7$	1.5	50 nm	150 (10 C)	1000 cycles (10 C, 75%)	[S31]

Supplementary References

[S1] L. Perfler, V. Kahlenberg, C. Wikete, D. Schmidmair, M. Tribus, R. Kaindl, Nanoindentation, High-Temperature Behavior, and Crystallographic/Spectroscopic Characterization of the High-Refractive-Index Materials $TiTa_2O_7$ and $TiNb_2O_7$, Inorg. Chem. 54 (2015) 6836-48.

[S2] C. Yang, S. Deng, C. Lin, S. Lin, Y. Chen, J. Li, H. Wu, Porous $TiNb_{24}O_{62}$ microspheres as high-performance anode materials for lithium-ion batteries of electric vehicles, Nanoscale 8 (2016) 18792-18799.

[S3] G. Liu, L. Zhao, R. Sun, W. Chen, M. Hu, M. Liu, X. Duan, T. Zhang, Mesoporous $TiNb_2O_7$ microspheres as high performance anode materials for lithium-ion batteries with high-rate capability and long cycle-life, Electrochim. Acta 259 (2018) 20-27.

[S4] K. J. Griffith, A. C. Forse, J. M. Griffin, C. P. Grey, High-Rate Intercalation without Nanostructuring in Metastable Nb_2O_5 Bronze Phases, J. Am. Chem. Soc. 138 (2016) 8888-99.

[S5] J. Hu, J. Li, K. Wang, H. Xia, Self-assembly Nb_2O_5 microsphere with hollow and carbon coated structure as high rate capability lithium-ion electrode materials, Electrochim. Acta 331 (2020) 135364.

[S6] Y. Li, S. Wang, Y.-B. He, L. Tang, Y. V. Kaneti, W. Lv, Z. Lin, B. Li, Q.-H. Yang, F. Kang, Li-ion and Na-ion transportation and storage properties in various sized TiO_2 spheres with hierarchical pores and high tap density, J. Mater. Chem. A 5 (2017) 4359-4367.

[S7] T. Lan, T. Wang, W. Zhang, N.-L. Wu, M. Wei, Rutile TiO_2 mesocrystals with tunable subunits as a long-term cycling performance anode for sodium-ion batteries, J. Alloy. Compd. 699 (2017) 455-462.

[S8] G. Liu, H.-H. Wu, Q. Meng, T. Zhang, D. Sun, X. Jin, D. Guo, N. Wu, X. Liu, J.-K. Kim, Role of the anatase/TiO_2(B) heterointerface for ultrastable high-rate lithium and sodium energy storage performance, Nanoscale Horiz. 5 (2020) 150-162.

[S9] J. Gao, J. Ying, C. Jiang, C. Wan, High-density spherical $Li_4Ti_5O_{12}$/C anode material with good rate capability for lithium ion batteries, J. Power Sources 166 (2007) 255–259.

[S10] H.-G. Jung, J. Kim, B. Scrosati, Y.-K. Sun, Micron-sized, carbon-coated $Li_4Ti_5O_{12}$ as high power anode material for advanced lithium batteries, J. Power Sources 196 (2011) 7763-7766.

[S11] L. Zhao, Y. S. Hu, H. Li, Z. Wang, L. Chen, Porous $Li_4Ti_5O_{12}$ coated with N-doped carbon from ionic liquids for Li-ion batteries, Adv. Mater. 23 (2011) 1385-8.

[S12] A. Nugroho, K. Y. Chung, J. Kim, A Facile Supercritical Alcohol Route for Synthesizing Carbon Coated Hierarchically Mesoporous $Li_4Ti_5O_{12}$ Microspheres, J. Phys. Chem. C 118 (2013) 183-193.

[S13] M. Odziomek, F. Chaput, A. Rutkowska, K. Swierczek, D. Olszewska, M. Sitarz, F. Lerouge, S. Parola, Hierarchically structured lithium titanate for ultrafast charging in long-life high capacity batteries, Nat. Commun. 8 (2017) 15636.

[S14] Xingneng group http://www.nem-cn.com/.

[S15] M. Saito, Y. Nakano, M. Takagi, N. Honda, A. Tasaka, M. Inaba, Improvement of tap density of TiO_2(B)

powder as high potential negative electrode for lithium ion batteries, J. Power Sources 244 (2013) 50-55.

[S16] Better our world http://www.btrchina.com/product/79.html.

[S17] H. Sun, L. Mei, J. Liang, Z. Zhao, C. Lee, H. Fei, M. Ding, J. Lau, M. Li, C. Wang, X. Xu, G. Hao, B. Papandrea, I. Shakir, B. Dunn, Y. Huang, X. Duan, Three-dimensional holey-graphene/ niobia composite architectures for ultrahigh-rate energy storage, Science 356 (2017) 599–604.

[S18] H.-G. Jung, S.-T. Myung, C. S. Yoon, S.-B. Son, K. H. Oh, K. Amine, B. Scrosati, Y.-K. Sun, Microscale spherical carbon-coated $Li_4Ti_5O_{12}$ as ultra high power anode material for lithium batteries, Energy. Environ. Sci. 4 (2011).

[S19] L. Sun, J. Wang, K. Jiang, S. Fan, Mesoporous $Li_4Ti_5O_{12}$ nanoclusters as high performance negative electrodes for lithium ion batteries, J. Power Sources 248 (2014) 265-272.

[S20] C. Wang, S. Wang, L. Tang, Y.-B. He, L. Gan, J. Li, H. Du, B. Li, Z. Lin, F. Kang, A robust strategy for crafting monodisperse $Li_4Ti_5O_{12}$ nanospheres as superior rate anode for lithium ion batteries, Nano Energy 21 (2016) 133-144.

[S21] C. Wang, S. Wang, Y.-B. He, L. Tang, C. Han, C. Yang, M. Wagemaker, B. Li, Q.-H. Yang, J.-K. Kim, F. Kang, Combining Fast Li-Ion Battery Cycling with Large Volumetric Energy Density: Grain Boundary Induced High Electronic and Ionic Conductivity in $Li_4Ti_5O_{12}$ Spheres of Densely Packed Nanocrystallites, Chem. Mater. 27 (2015) 5647−5656.

[S22] S.-L. Chou, J.-Z. Wang, H.-K. Liu, S.-X. Dou, Rapid Synthesis of $Li_4Ti_5O_{12}$ Microspheres as Anode Materials and Its Binder Effect for Lithium-Ion Battery, J. Phys. Chem. C 115 (2011) 16220-16227.

[S23] H. Liu, Z. Bi, X.-G. Sun, R. R. Unocic, M. P. Paranthaman, S. Dai, G. M. Brown, Mesoporous TiO_2-B Microspheres with Superior Rate Performance for Lithium Ion Batteries, Adv. Mater. 23 (2011) 3450-3454.

[S24] J. Y. N. S.R. Sivakkumar, A.G. Pandolfo, Rate capability of graphite materials as negative electrodes in lithium-ion capacitors, Electrochim. Acta 55 (2010) 3330–3335.

[S25] K. Tang, X. Mu, P. A. van Aken, Y. Yu, J. Maier, "Nano-Pearl-String" $TiNb_2O_7$ as Anodes for Rechargeable Lithium Batteries, Adv. Energy Mater. 3 (2013) 49-53.

[S26] S. Deng, H. Zhu, G. Wang, M. Luo, S. Shen, C. Ai, L. Yang, S. Lin, Q. Zhang, L. Gu, B. Liu, Y. Zhang, Q. Liu, G. Pan, Q. Xiong, X. Wang, X. Xia, J. Tu, Boosting fast energy storage by synergistic engineering of carbon and deficiency, Nat. Commun. 11 (2020) 132.

[S27] H. Kim, Y. Lee, D. Byun, W. Choi, $TiNb_2O_7$ microsphere anchored by polydopamine-modified graphene oxide as a superior anode material in lithium-ion batteries, Int. J. Energy Res. 44 (2020) 4986-4996.

[S28] H. Li, L. Shen, G. Pang, S. Fang, H. Luo, K. Yang, X. Zhang, $TiNb_2O_7$ nanoparticles assembled into hierarchical microspheres as high-rate capability and long-cycle-life anode materials for lithium ion batteries, Nanoscale 7 (2015) 619-24.

[S29] Q. Cheng, J. Liang, Y. Zhu, L. Si, C. Guoa, Y. Qian, Bulk $Ti_2Nb_{10}O_{29}$ as long-life and high-power Li-ion

battery anodes, J. Mater. Chem. A 2 (2014) 17258.

[S30] Z. Yao, X. Xia, Y. Zhang, D. Xie, C. Ai, S. Lin, Y. Wang, S. Deng, S. Shen, X. Wang, Y. Yu, J. Tu, Superior high-rate lithium-ion storage on $Ti_2Nb_{10}O_{29}$ arrays via synergistic TiC/C skeleton and N-doped carbon shell, Nano Energy 54 (2018) 304-312.

[S31] S. Lou, X. Cheng, Y. Zhao, A. Lushington, J. Gao, Q. Li, P. Zuo, B. Wang, Y. Gao, Y. Ma, C. Du, G. Yin, X. Sun, Superior performance of ordered macroporous $TiNb_2O_7$ anodes for lithium ion batteries: Understanding from the structural and pseudocapacitive insights on achieving high rate capability, Nano Energy 34 (2017) 15-25.